applied sciences

MDPI

Article

Study of Eco-Friendly Belite-Calcium Sulfoaluminate Cements Obtained from Special Wastes

Antonio Telesca [1], Thomas Matschei [2] and Milena Marroccoli [1,*]

[1] Scuola di Ingegneria, Università degli Studi della Basilicata, Viale dell'Ateneo Lucano 10, 85100 Potenza, Italy; antonio.telesca@unibas.it

[2] Institute of Building Materials Research, RWTH Aachen University, Schinkelstr. 3, D-52062 Aachen, Germany; matschei@ibac.rwth-aachen.de

* Correspondence: milena.marroccoli@unibas.it

Received: 15 November 2020; Accepted: 30 November 2020; Published: 3 December 2020

Abstract: Belite-calcium sulfoaluminate (BCSA) cements are special binders obtained from non-Portland clinkers; they have become increasingly more important due to their environmental impact during the manufacturing process compared to Portland cements, such as lower energy consumption and CO_2 emissions. The aim of this paper was to assess the possible use of titanogypsum (T) and water potabilization sludge (W) to reduce the amount of natural raw materials (natural gypsum and clay, respectively) used in the production of BCSA cements. Three BCSA clinker generating raw mixes, containing T and/or W, and a reference mix based only on natural materials (limestone, clay, bauxite and natural gypsum) were heated in an electric furnace at temperatures ranging from 1200 to 1350 °C. Quantitative X-ray diffraction (XRD) analysis of the burnt products showed high conversion of reactants towards the main hydraulically active BCSA clinkers components (C_2S and $C_4A_3\$$), particularly at temperatures of 1300 and 1350 °C. Isothermal calorimetric measurements, differential thermal–thermogravimetric and XRD analyses as well as porosimetric measurements showed that all BCSA cements, from mixing the clinkers (at optimum temperatures) with commercial anhydrite, exhibited similar hydration behavior.

Keywords: sustainability; titanogypsum; water potabilization sludge; synthesis; belite-calcium sulfoaluminate cements; hydration

1. Introduction

The cement industry consumes huge amounts of natural raw materials and fuels, mainly fossil fuels and pet coke. It is one of the main contributors to climate change due to greenhouse gas emissions, mainly CO_2. In 2018, global cement production was about 3.99 billion tonnes, accounting for about 8% of all anthropogenic carbon dioxide emissions [1]. Ordinary Portland cement (OPC), a blend of clinker (about 95%) and gypsum, is the most used binder in the world. OPC clinker is usually obtained by heating a mixture (raw meal) of limestone (L, 80% by mass) [2] and clay (C) in a rotary kiln at about 1500 °C. According to [3], about 0.83 kg of CO_2 is released from the production of 1 kg of OPC; it is generated from both L thermal decomposition (about 60% of the total CO_2 emissions) and fuel combustion [4,5].

To reduce its carbon footprint, the cement industry is exploring how to manufacture OPC with less impact on the environment through a switch to: (I) alternative fuels, (II) reduction in thermal energy demand, (III) use of non-carbonated CaO sources instead of L, (IV) decrease in clinker to cement ratio, (V) application of carbon capture and storage technologies to cement plants [6], and (VI) development of low-CO_2 non-Portland binders (e.g., alkali-activated, Mg-based cements, calcium sulfoaluminate (CSA) and belite–CSA (BCSA) binders) [7–25].

BCSA cements represent a promising alternative to OPC as they exhibit comparable physical and mechanical properties [26–41]. The technical behavior of BCSA cements mostly depends on the ability of C_2S and $C_4A_3\$$ (their main components) to generate, upon hydration, CSH (calcium silicate hydrates, at medium and longer periods) and $C_6A\$_3H_{32}$ (ettringite, at early ages), respectively. They are also characterized by eco-friendly features due to: (a) a lower synthesis temperature, (b) a reduced amount of L in the clinker generating raw mixture, (c) a decreased specific fuel consumption, and (d) easier clinker grindability [25,29]. All these features allow a reduction in CO_2 of up to 30% [25].

BCSA cements are obtained at temperatures ranging between 1250 and 1350 °C by burning a raw meal composed of L, C, natural gypsum (G) and bauxite (B); natural raw materials can be effectively replaced by special wastes that are often difficult to reuse and/or landfill (e.g., blast-furnace slag, coal combustion ash from both traditional combustors and fluidized bed reactors, red mud, alumina powders, phosphogypsum and flue gas desulfurization gypsum). In particular, the use of alumina-rich wastes can lower the manufacturing costs of BCSA cements mainly depending on the use of the "expensive" bauxite [42–51].

Water potabilization sludge (W) is a clayish residue produced in conventional drinking water treatment plants where suspended particles are eliminated by means of coagulation and flocculation processes using aluminum salts-based coagulants [52]. High quantities of sludge, representing about 1–5% of the total untreated water amount, are generated; therefore, huge amounts of W are produced worldwide (~10,000 ton/day) and most of them are landfilled. Until now, W has been used in the production of bricks, ceramics, lightweight aggregates and as an alternative raw material in the Portland cement manufacturing process [53].

Titanogypsum (T) is a sulfate-rich waste deriving from the production of titanium dioxide pigment, which is generally used in paints, plastics, papers, coatings, cosmetics, etc. The global production of TiO_2 pigments accounts for about 4 million tonnes/year; about one-half of TiO_2-based pigments is produced by the sulfate process, the other half by the chloride route. Only the former generates T; depending on the quality of the titanium-bearing ore, red T or white T can be obtained. So far, both kinds of T are only partly used in the Portland cement industry and in the production of plasterboard.

This paper aimed to investigate the synthesis process and hydration behavior of three laboratory-made BCSA cements. BCSA clinkers were obtained from raw meals containing T and/or W as total substitutes for G and C, respectively, at temperatures comprised in the range of 1200–1350 °C. A reference mixture based on L, B, C and G underwent the same thermal treatments.

In this paper, novel residues have been investigated for the manufacture of BCSA cements; both W and T are very interesting as their utilization permits the saving of natural materials and avoids the landfilling of waste. In particular, the use of W allows us to completely replace bauxite as an Al_2O_3 source.

Quantitative X-ray diffraction (QXRD) analysis was used to evaluate the reactivity of all BCSA clinker-generating raw mixes. The hydration behavior of BCSA cements, obtained by mixing the clinkers heated at the best synthesis temperatures with commercial anhydrite, was investigated for different curing times using differential thermal–thermogravimetric (DT–TG) and XRD analyses as well as isothermal calorimetry and mercury intrusion porosimetry (MIP).

2. Materials and Methods

2.1. Raw Materials and Proportioning of CSA Clinker-Generating Raw Mixtures

The chemical compositions of the natural materials (L, B, C, and G) and the special wastes (T and W) used in this investigation are listed in Table 1. The L, B, C and G samples were supplied by an Italian cement manufacturer. T and W came from an international titanium dioxide pigment company and a water treatment plant of the "Camastra" artificial reservoir located in the Basilicata Region (Italy), respectively.

Table 1. Chemical analysis of the natural and waste raw materials, wt%.

	L	B	G	C	T	W
CaO	55.20	-	34.08	12.20	30.89	4.95
SiO_2	-	7.20	0.51	54.60	1.00	37.71
Al_2O_3	-	56.30	0.71	10.00	0.52	27.52
Fe_2O_3	-	6.30	0.30	3.70	2.24	2.37
SO_3	-	-	44.37	-	40.13	0.53
Others	1.40	2.70	0.81	5.20	3.54	4.70
l.o.i. *	43.40	27.50	19.02	14.30	21.82	22.12

* loss on ignition at 950 ± 25°C.

All the samples were first dried in an electric oven at 105 °C until a constant mass value was reached and then, finely pulverized in a Fritsch Pulverisette 6 (FP6) laboratory planetary mill to pass through the 90 μm sieve.

Four BCSA clinker-generating raw mixtures (RM_R, RM_T, RM_W and RM_TW) were investigated: the first (RM_R) was based only on natural materials; the others contained T (RM_T) or W (RM_W) or both T and W together (RM_TW). The composition of raw mixtures was determined according to modified Bogue calculations (MBCs) [35]; it was assumed that C_2S, $C_4A_3\$$, C_4AF and C$ amounts were, respectively, comprised in the ranges 45–60%, 20–30%, 8–20% and 4–10%. A concentration value of free-CaO (C_f) lower than 1.5% was also considered. In order to obtain reactive belite in the cement clinkers, 1% by mass of B_2O_3 was added to the raw mixtures.

The proportion of raw meals and mineralogical compositions, estimated according to the MBCs, of the four clinkers (C_R, C_T, C_W and C_TW) are reported in Tables 2 and 3, respectively.

Table 2. Composition of the raw meals, wt%.

	L	B	G	C	T	W
RM_R	55.0	13.0	9.0	23.0	-	-
RM_T	55.0	12.0	-	23.0	10.0	-
RM_W	55.0	-	9.0	-	-	36.0
RM_TW	55.0	-	-	-	10.0	35.0

Table 3. Mineralogical compositions (estimated according to the modified Bogue calculations (MBCs)) of the clinkers, wt%.

	C_2S	$C_4A_3\$$	C_4AF	C$	C_f
C_R	57.5	25.4	7.6	4.4	1.6
C_T	57.6	23.5	8.3	4.9	1.9
C_W	58.8	28.2	4.0	4.4	0.7
C_WT	56.4	27.1	3.9	5.6	-

2.2. Burning of Raw Mixtures

Four 100 g batches of each clinker-generating raw mixture, placed in covered alumina crucibles to prevent sulfur emissions, were heated in an electric furnace at four different temperatures (1200, 1250, 1300 and 1350 °C, with an accuracy of ±2 °C) according the procedure reported in [8]. The resulting BCSA clinkers (65–70 g) were finely ground using a planetary mill to pass through the 90 μm sieve and then submitted to QXRD analysis in order to assess the best synthesis temperature to maximize the sum of C_2S and $C_4A_3\$$.

2.3. Preparation of BCSA Cements

BCSA cements were prepared by grinding the four clinkers heated at the best synthesis temperatures with commercial anhydrite (containing 96.6% by mass of C$) using a mill to pass

through the 90 μm sieve. The specific surfaces of the clinkers (according to EN 196-6 (CEN, 2018)) were in the range 4600 ± 100 cm^2/g. The amount of anhydrite to be added was determined by subtracting the quantity of C$ already present in the BCSA clinkers from the value necessary for the complete reaction of C_4A_3\$ to ettringite according to the following reaction [15]:

$$C_4A_3\$+2C\$+38H \Rightarrow C_6A\$H_{32} +2AH_3 \quad (1)$$

Therefore, the resulting BCSA cements were indicated using the same symbols used for their generating raw mixtures (CEM_R, CEM_T, CEM_W, CEM_TW); their mix design is summarized in Table 4.

Table 4. Mix design (g/100 g cement) of the investigated systems, wt%.

	CEM_R	CEM_T	CEM_W	CEM_TW
BCSA clinker	93.1	92.5	90.8	88.6
Anhydrite	6.9	7.5	9.2	11.4
Total	100.0	100.0	100.0	100.0

2.4. Hydration Procedure

Cement powders were hydrated using a water/cement ratio equal to 0.5 by mass. The paste samples were cast into small cylindrical molds (15 mm high and 30 mm diameter) and put inside a thermostatic bath (at 20 °C and 95% relative humidity) for aging periods ranging from 4 h up to 90 days.

At the end of each aging period, the specimens were broken in half: one part was submitted to mercury intrusion porosimetry (MIP) characterizations, the other was gently pulverized for DT–TG and XRD measurements. Both components, namely hardened fragments and fine powder, were treated with acetone (to stop hydration) and diethyl ether (to remove water) and finally, stored in a desiccator containing silica gel and soda lime (to ensure protection against H_2O and CO_2, respectively)

2.5. Characterization Techniques

2.5.1. X-ray Fluorescence Analysis

X-ray fluorescence (XRF) analysis was used to determine the chemical composition of the raw materials. A wave dispersive Bruker Explorer S4 apparatus (maximum power = 1 kW; LiF200, PET, OVO-55, OVO-B as analyzing crystals) was used. Loss on ignition (l.o.i.) was determined according to EN 196-2 [54]. One gram (1 ± 0.05 g) of each material was calcined at 950 ± 25 °C for 15 min; calcination was repeated until a constant weight was achieved.

2.5.2. DT–TG Analysis

A simultaneous DT–TG apparatus (NETZSCH-Tasc 414/3), operating between room temperature and 1000 °C with a heating rate of 10 °C min^{-1} in 150 μL alumina crucibles, was employed to evaluate BCSA cements' hydration products (at 4 h, 2, 28 and 90 d). TG analysis was also used to quantitatively determine chemically bound water [55] on samples hydrated at 4 h, 2, 28 and 90 d.

2.5.3. XRD Analysis

XRD analysis was performed to determine the mineralogical composition of both the CSA clinkers and the hydrated cement pastes (at 4 h, 7 and 28 d). A Bruker D4 Endeavor X-ray diffractometer using CuKα radiation and a Linx Eye dispersive detector were used. The samples were scanned at a step size of 0·02°2θ for 45 min between 8° and 55°2θ. Rietveld refinement of the XRD patterns was performed using the TOPAS 2.0 package.

2.5.4. Isothermal Calorimetry

Isothermal calorimetry, using a Calmetrix n I-cal flex calorimeter, was applied to measure the heat release during hydration of cement pastes (w/c = 0.5) up to 14d. Measurements were taken at room temperature. In total, 20 g of each cement paste was externally mixed for 30 s using a Stuart SA 6 variable speed vortex mixer with a mixing speed of 2500 rpm.

2.5.5. Mercury Intrusion Porosimetry (MIP)

The porosity measurements were taken using a Thermo-Finnigan Pascal 240 Series mercury porosimeter (maximum pressure, 200 MPa) equipped with a low-pressure unit (140 Series) able to generate a high vacuum level (10 Pa) and operate between 100 and 400 kPa. MIP measurements were carried out on fragments hydrated for 7, 28 and 90 days. MIP was employed to better understand the properties of the hydrated binders through the evaluation of microstructure development over time.

3. Results and Discussion

3.1. Synthesis of BCSA Clinkers

The main BCSA clinkers mineralogical phases (taken at 1200, 1250, 1300 and 1350 °C) are displayed in Table 5. From an overall examination of the QXRD clinker data, it could be argued that, at all investigated temperatures, I) C_2S and $C_4A_3\$$ are the main burning products and II) the conversion of reactants is complete; in addition, the best results were obtained at 1300 °C for RM_W and at 1350 °C for the other mixtures. Furthermore, tricalcium aluminate (C_3A) brownmillerite (C_4AF), and periclase (MgO) were observed in all the clinkers as secondary components; anhydrite (C$), and CaO_f were identified only as minor components.

Table 5. Mineralogical composition of BCSA clinkers determined according to Rietveld, wt%.

	β-C_2S	**$C_4A_3\$$ ***	**C_3A**	**C_4AF**	**Others**
C_R					
1200 °C	47.2	19.7	9.1	0.9	23.1
1250 °C	42.0	16.7	10.4	3.4	27.5
1300 °C	54.3	16.7	9.4	3.9	15.7
1350 °C	60.0	16.7	10.9	4.4	8.0
C_T					
1200 °C	42.3	16.7	10.2	3.2	27.6
1250 °C	38.1	18.8	11.0	5.7	26.4
1300 °C	40.4	20.7	8.6	6.7	23.6
1350 °C	53.3	19.7	5.3	8.1	13.6
C_W					
1200 °C	42.8	22.0	11.0	2.0	22.2
1250 °C	45.6	22.6	10.9	3.1	17.8
1300 °C	54.3	22.8	10.6	6.6	5.7
1350 °C	46.9	24.5	9.6	4.8	14.2
C_TW					
1200 °C	44.5	19.7	8.6	0.8	26.4
1250 °C	34.6	30.5	15.2	4.7	15.0
1300 °C	36.8	29.9	14.1	5.1	14.1
1350 °C	45.7	28.9	13.8	9.0	12.6

* Orthorhombic + cubic crystalline structures.

QXRD results showed that Al_2O_3, not involved in the formation of $C_4A_3\$$, was more inclined to give C_3A instead of C_4AF. In addition, the amounts of sulfates (namely those present in both $C_4A_3\$$ and C$) were lower than those estimated using the Bogue equations; this difference was presumably related to the volatilization phenomena involving part of the sulfur oxides. On the whole, these results

emphasize the active role played by the sources of silicate, alumina and sulfate supplied by the wastes analyzed (T and W), which reacted as the corresponding natural materials. Figure 1 reports the XRD patterns for the four mixes heated at their best synthesis temperature.

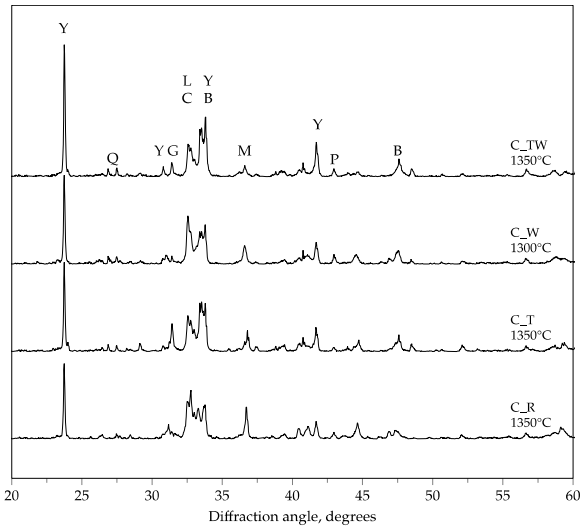

Figure 1. XRD patterns for C_R, C_T, C_W and C_TW heated at the best synthesis temperature (B = C_4AF, C = C_3A, G = C_2AS, Y = $C_4A_3\$$, L = β-C_2S, M = $C_{12}A_7$, P = MgO, Q = SiO_2).

3.2. Hydration of BCSA Cements

Figure 2 shows the DT–TG thermograms for the four BCSA cements hydrated for periods between 4 h and 90 days. With DT–TG temperature increase, three different endothermal effects were identified at 93 ± 9 °C, 149 ± 9 °C and 277 ± 5 °C, and were attributed, in this order, to the following hydration products [55]: CSH, $C_6A\$_3H_{32}$ and AH_3, respectively. Moreover, no significant effects were found above 500 °C.

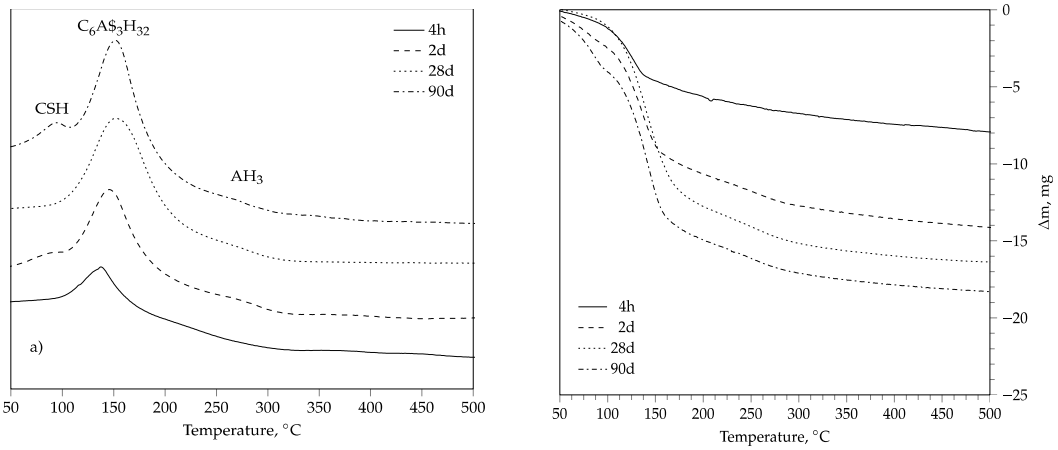

Figure 2. *Cont.*

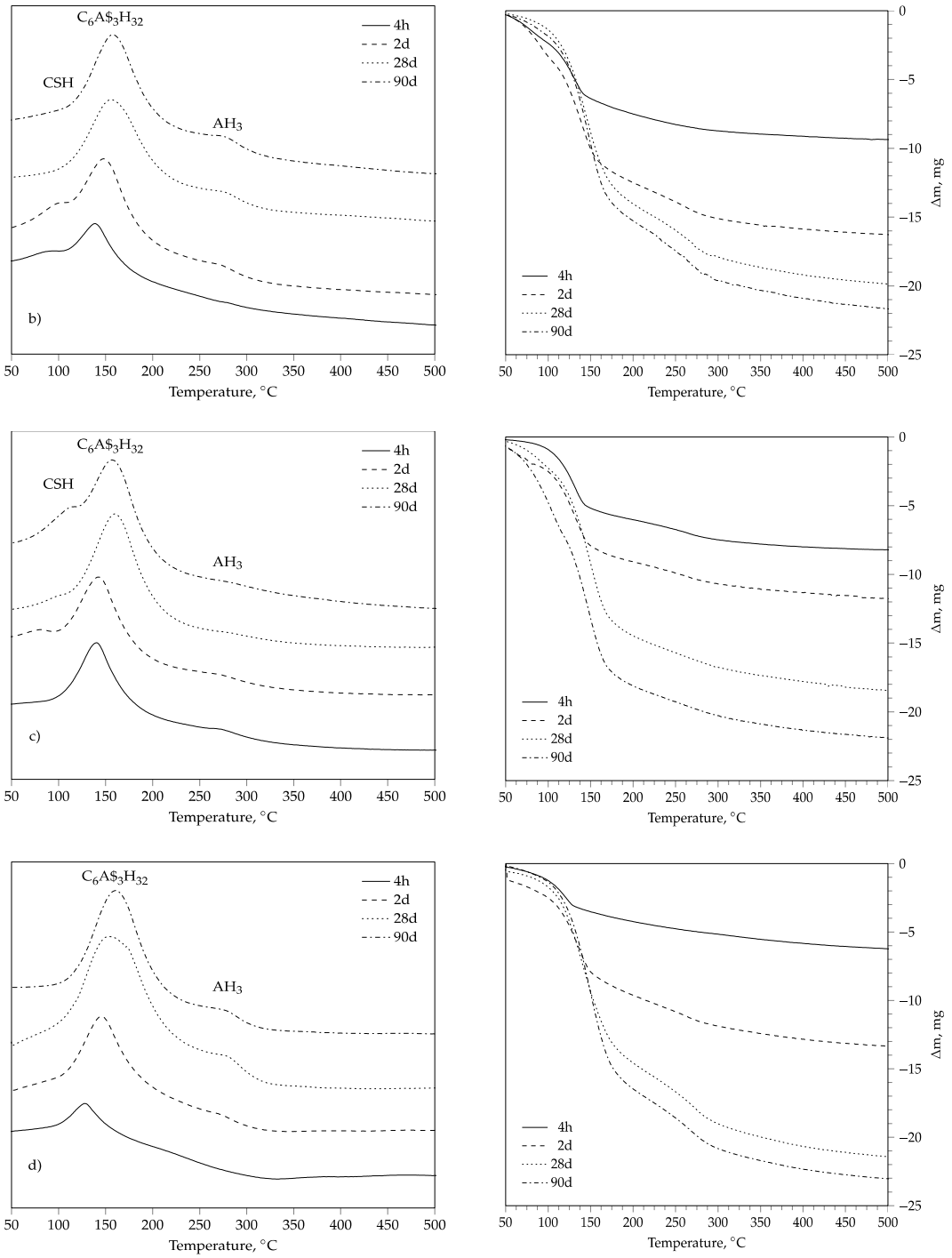

Figure 2. Differential thermal (DT, **left**)–thermogravimetric (TG, **right**) thermograms for CEM_R (**a**), CEM_T (**b**), CEM_W (**c**) and CEM_TW (**d**) cured at various ages.

On the whole, the DT results reveal the presence of $C_6A\$_3H_{32}$ and AH_3 for all the curing periods, apart from the pastes based on CEM_R and CEM_TW, where aluminum hydroxide materializes after 2 days of hydration; furthermore, both $C_6A\$_3H_{32}$ and AH_3 concentrations increased with aging time. Calcium silicate hydrates were not always distinguished, as their DT effect was overlapped by the ettringite (E) peak. Monosulfate could not be clearly detected owing to the overlap of the E signal.

TG curves show the mass loss related to dehydration and dehydroxylation phenomena involving CSH, ettringite and monosulfate (from room temperature to ~200 °C) as well as aluminum hydroxide (from 200 to ~300 °C), respectively. The higher weight loss values up to about 200 °C are related to

the formation of the main hydration products, namely CSH and ettringite; moreover, as curing time increases, their amount increases.

The BCSA cements' hydration rates were also evaluated using the amount of chemically bound water (Figure 3) calculated from the mass loss values from TG analyses (Figure 2).

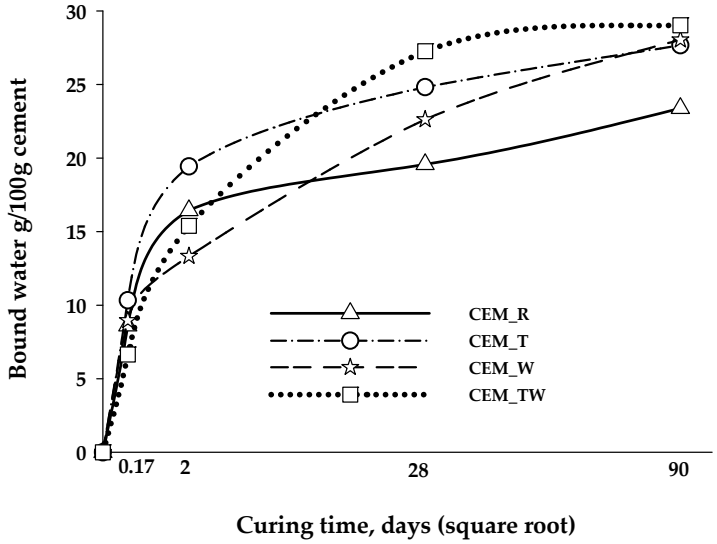

Figure 3. Bound water as determined by TG up to 90 days of hydration (normalized to BCSA cement) for CEM_R, CEM_T, CEM_W and CEM_TW plotted against curing time.

Figure 3 shows that the four systems followed a similar trend in terms of the evolution of the hydration process. With the exception of the reference system, which displayed the worst hydration behavior, the other binders reached comparable bound water content after 90 days of curing.

The hydration process was also investigated using XRD analysis. XRD patterns (for samples hydrated at 4 h, 7 and 28 days) are shown in Figure 4, where only the most significant phases are indicated; they allowed for the detection of: (a) the consumption of reactants, (b) the presence of inert phases, and (c) the development of hydration products (mainly ettringite). The absence of CSH and AH_3 among the crystalline phases detected using XRD analysis is associated with their amorphous nature. As for the DT thermograms, it has been found that as curing time increases, the ettringite peaks increase at the expense of both the ye'elimite and anhydrite peaks. Weak peaks for monosulfate were detectable in the systems CEM_R, CEM_W and CEM_TW at 7 days of curing, and at 28 days for the CEM_T systems. Furthermore, CEM_TW hydrated more slowly than the other systems. XRD patterns at 28 days still revealed the presence of some unconsumed reactants such as ye'elimite and anhydrite.

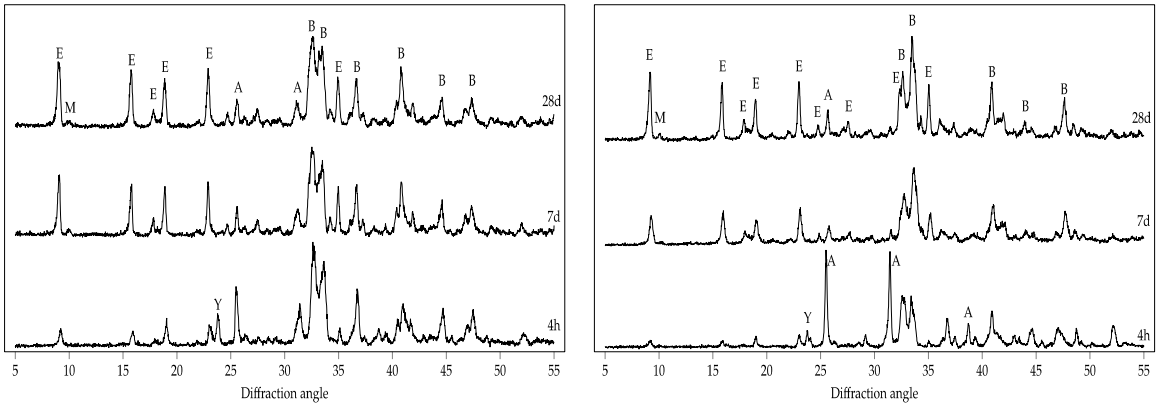

Figure 4. *Cont.*

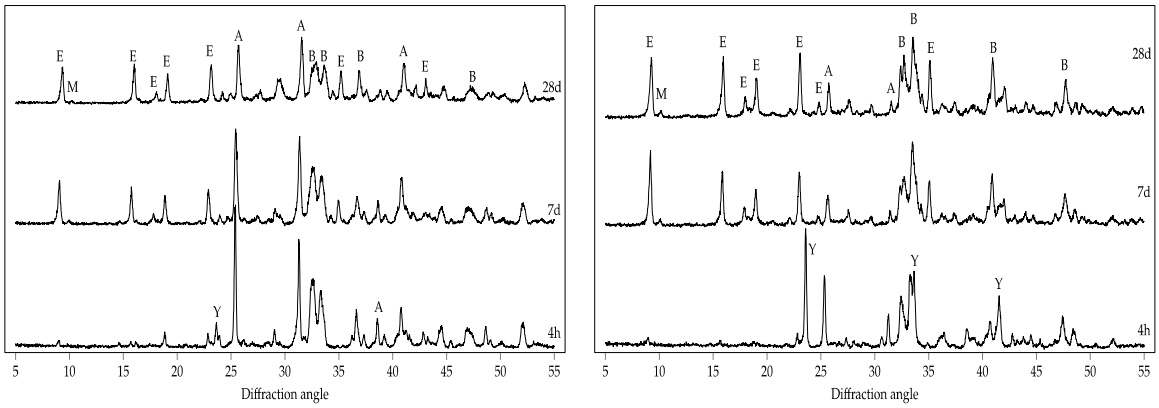

Figure 4. XRD patterns for CEM_R (**top left**) and CEM_T (**top right**); CEM_W (**bottom left**) and CEM_TW (**bottom right**) cured at various ages. (A, anhydrite; B, belite; E, ettringite; M, monosulfate).

Figure 5 displays the results of the isothermal calorimetry measurements of the four cements. CEM_TW, namely the system with the highest amount of $C_4A_3\$$, showed the highest cumulative heat release over 14 days of hydration. It is worth noting that, compared to the other systems, the main hydration reactions were significantly slower and only started after ~24 h, which also agrees closely with the DT–TG data. Another interesting feature was observed for CEM_R, which exhibited a second acceleration of the hydration reactions after about 9 days. The reason for this behavior is most likely related to a change in the resulting solid phase equilibria, which may have caused changes in the pore solution chemistry.

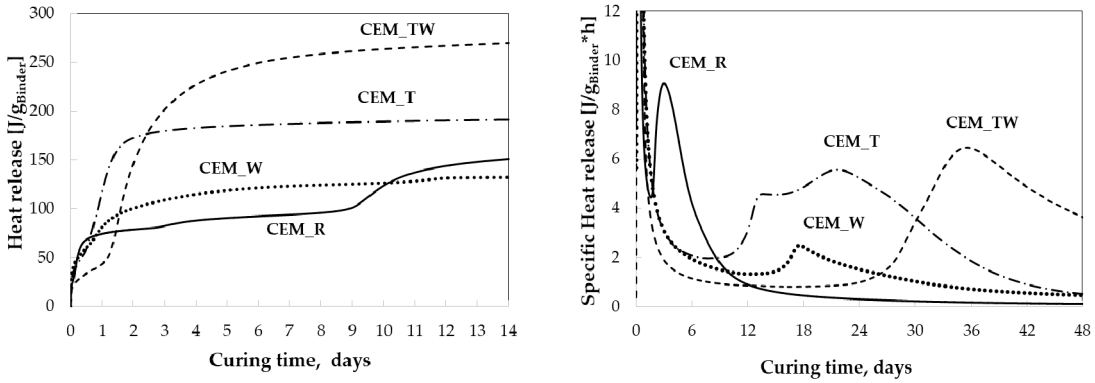

Figure 5. Cumulative (**left**) and specific (**right**) heat release of BCSA cement samples.

The porosimetric characteristics of OPC pastes have been widely studied and extensively reported in the scientific and technical literature [56–58]; it is well known that total porosity, threshold pore width and cumulative pore volume decrease as curing times increase [18]. At early ages, the differential curves show an initial sharply defined peak, indicating a unimodal pore size distribution, centered on the lowest width of pore necks connecting a continuous system. At longer curing times, a second peak appears, corresponding to the pressure required to break through the blockages formed by the hydration products which isolate the interior pore space.

Figure 6 reports both cumulative and derivative plots for intruded Hg volume vs. pore radius for CEM_R at various curing times. For periods between 7 and 90 days, the pore size distribution was unimodal, with a threshold pore width ranging from about 300 to 15 nm. During the same period, the cumulative pore volume significantly reduces (from about 215 to 130 mm^3/g).

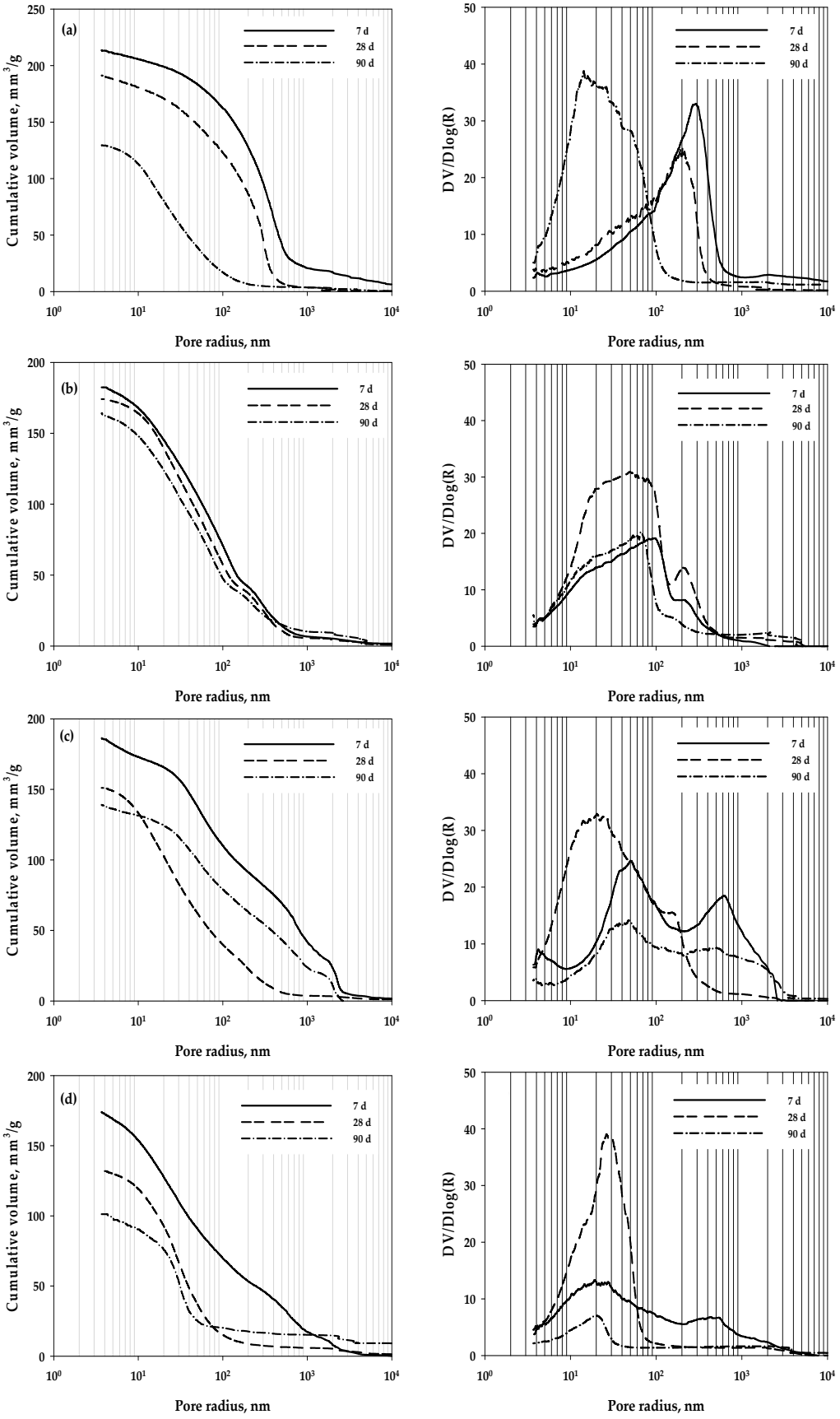

Figure 6. Cumulative (**left**) and derivative (**right**) Hg volume vs. pore radius for CEM_R (**a**), CEM_T (**b**), CEM_W (**c**) and CEM_TW (**d**) cement pastes cured at various ages.

Compared to CEM_R, CEM_T always showed a bimodal pore size distribution. The peak oriented toward higher radii values varied in a small range, from 200 at 7 days to about 180 nm at 90 days; however, the second peak ranged from about 100 at 7 days to 35 nm at 90 days. The cumulative Hg volume for CEM_T comprised the small range of 180–165 mm^3/g.

Figure 6 displays both cumulative and derivative curves for CEM_W. At 7 days of aging, the pore size distribution was trimodal, with a pore radius equal to about 650, 50 and 4 nm. After longer curing periods, the pore size distribution became bimodal, with pore radii equal to about 550 and 45 nm at 28 days as well as 150 and 20 nm at 90 days; this was due to the shift of the smallest peak beyond the minimum detectable pore value by the porosimeter (3.6 nm). During the same period, the cumulative pore volume decreased from about 180 to 140 mm^3/g.

At 7 days of curing, the differential curve for CEM_TW exhibited two quite wide peaks centered at about 500 and 25 nm, respectively, indicating a bimodal pore size distribution. A unimodal pore size distribution was established over longer aging periods (peaks centered at about 25 and 20 nm, respectively, at 28 and 90 days). The cumulative pore volume appreciably reduced between 7 and 90 days (about 175 to 100 mm^3/g).

4. Conclusions

Titanogypsum (T) and water potabilization sludges (W) can, respectively, be used as suitable substitutes for natural gypsum and clay in belite-calcium sulfoaluminate (BCSA) clinker-generating raw mixes. The best results were obtained at 1300 °C (for the raw meal containing W) and at 1350 °C (for mixes containing only natural raw materials and for those containing T or both T and W) for selectivity of reactants towards the main hydraulically active components of BCSA cement (C_2S and $C_4A_3\$$).

Isothermal calorimetry (up to 14 days) and differential thermal–thermogravimetric analyses indicated some differences in the hydration kinetics, associated with the kind of sulfate and clayish sources used for the synthesis of BCSA clinkers. In addition, BCSA cements containing T (CEM_T) and/or W (CEM_TW, CEM_W) displayed faster hydration kinetics than the reference system, while CEM_TW and CEM_T exhibited the highest hydration heat for the systems studied. As far as the ability of generating hydration products is concerned, the experimental results revealed an almost analogous tendency; however, at the longest curing periods, the best results were from the waste-based cements.

The behavior of BCSA cements can be improved using industrial wastes in place of raw materials, reducing the need for natural materials and landfill waste. The use of W in the clinker generating raw mix, averting the utilization of bauxite as the alumina source, could reduce BCSA manufacturing costs. Nonetheless, additional studies are necessary to understand the impact of the use of alternative raw materials and their minor components on hydration behavior.

Author Contributions: A.T.: conceptualization; methodology; formal analysis; investigation; data curation; writing—original draft preparation; writing—review and editing. T.M.: methodology; formal analysis; investigation; writing—review and editing. M.M.: conceptualization; methodology; formal analysis; investigation; data curation; writing—original draft preparation; writing—review and editing. All authors have read and agreed to the published version of the manuscript.

Funding: This research received no external funding.

Conflicts of Interest: The authors declare no conflict of interest.

References

1. Activity Report 2019. The European Cement Association. Available online: https://cembureau.eu/media/clkdda45/activity-report-2019.pdf (accessed on 26 November 2020).
2. Tregambi, C.; Solimene, R.; Montagnaro, F.; Salatino, P.; Marroccoli, M.; Ibrid, N.; Telesca, A. Solar-driven production of lime for ordinary Portland cement formulation. *Sol. Energy* **2018**, *173*, 759–768. [CrossRef]
3. Barcelo, L.; Kline, J.; Walenta, G.; Gartner, E. Cement and carbon emissions. *Mater. Struct.* **2014**, *47*, 1055–1065. [CrossRef]

4. Xu, D.; Cui, Y.; Li, H.; Yang, K.; Xu, W.; Chen, Y. On the future of Chinese cement industry. *Cem. Concr. Res.* **2015**, *78*, 2–13. [CrossRef]
5. Telesca, A.; Marroccoli, M.; Ibris, N.; Lupiáñez, C.; Díez, L.I.; Romeo, L.M.; Montagnaro, F. Use of oxyfuel combustion ash for the production of blended cements: A synergetic solution toward reduction of CO_2 emissions. *Fuel Proc. Technol.* **2017**, *156*, 211–220. [CrossRef]
6. Schneider, M. The cement industry on the way to a low-carbon future. *Cem. Concr. Res.* **2019**, *124*, 105792. [CrossRef]
7. Shi, C.; Qu, B.; Provis, J.L. Recent progress in low-carbon binders. *Cem. Concr. Res.* **2019**, *122*, 227–250. [CrossRef]
8. Gartner, E.; Sui, T. Alternative cement clinkers. *Cem. Concr. Res.* **2018**, *114*, 27–39. [CrossRef]
9. Luukkonen, T.; Abdollahnejad, Z.; Yliniemi, J.; Kinnunen, P.; Illikainen, M. One-part alkali-activated materials: A review. *Cem. Concr. Res.* **2018**, *103*, 21–34. [CrossRef]
10. Myers, R.J.; Lothenbach, B.; Bernal, S.A.; Provis, J.L. Thermodynamic modelling of alkali-activated slag cements. *Appl. Geochem.* **2015**, *61*, 233–247. [CrossRef]
11. Provis, J.L.; van Deventer, J.S.J. *Alkali-Activated Materials: State-of-the-Art Report, RILEM TC 224-AAM.*; Springer/RILEM: Dordrecht, The Netherlands, 2014.
12. Dung, N.T.; Unluer, C. Development of MgO concrete with enhanced hydration and carbonation mechanisms. *Cem. Concr. Res.* **2018**, *103*, 160–169. [CrossRef]
13. Gomez, C.M.; de Oliveira, A.D.S. Chemical phases and microstructural analysis of pastes based on magnesia cement. *Constr. Build. Mater.* **2018**, *188*, 615–620. [CrossRef]
14. Walling, S.A.; Provis, J.L. Magnesia-based cements: A journey of 150 years, and cements for the future? *Chem. Rev.* **2016**, *116*, 4170–4204. [CrossRef] [PubMed]
15. Mobili, A.; Telesca, A.; Marroccoli, M.; Tittarelli, F. Calcium sulfoaluminate and alkali-activated fly ash cements as alternative to Portland cement: Study on chemical, physical-mechanical, and durability properties of mortars with the same strength class. *Constr. Build. Mater.* **2020**, *246*, 118436. [CrossRef]
16. Ben Haha, M.; Winnefeld, F.; Pisch, A. Advances in understanding ye'elimite-rich cements. *Cem. Concr. Res.* **2019**, *123*, 105778. [CrossRef]
17. Telesca, A.; Marroccoli, M.; Tomasulo, M.; Valenti, G.L.; Dieter, H.; Montagnaro, F. Low-CO_2 cements from fluidized bed process wastes and other industrial byproducts. *Combust. Sci. Technol.* **2016**, *188*, 492–503. [CrossRef]
18. Telesca, A.; Marroccoli, M.; Pace, M.L.; Tomasulo, M.; Valenti, G.L.; Monteiro, P.J.M. A hydration study of various calcium sulfoaluminate cements. *Cem. Concr. Comp.* **2014**, *53*, 224–232. [CrossRef]
19. Irico, S.; Gastaldi, D.; Canonico, F.; Magnacca, G. Investigation of the microstructural evolution of calcium sulfoaluminate cements by thermoporometry. *Cem. Concr. Res.* **2013**, *53*, 239–247. [CrossRef]
20. Winnefeld, F.; Lothenbach, B. Hydration of calcium sulfoaluminate cements—Experimental findings and thermodynamic modelling. *Cem. Concr. Res.* **2010**, *40*, 1239–1247. [CrossRef]
21. Selçuk, N.; Soner, I.; Selçuk, E. Synthesis of special cement with fluidized bed combustion ashes. *Adv. Cem. Res.* **2010**, *22*, 107–113. [CrossRef]
22. Marroccoli, M.; Pace, M.L.; Telesca, A.; Valenti, G.L. Synthesis of calcium sulfoaluminate cements from Al_2O_3-rich by-products from aluminium manufacture. In Proceedings of the 2nd International Conference on Sustainable Construction Materials and Technologies, Ancona, Italy, 28–30 June 2010; Zachar, J., Claisse, P., Naik, T.R., Ganjiam, E., Eds.; UWM Center for By-Products Utilization: Milwaukee, WI, USA, 2010.
23. Marroccoli, M.; Montagnaro, F.; Telesca, A.; Valenti, G.L. Environmental implications of the manufacture of calcium sulfoaluminate-based cements. In Proceedings of the 2nd International Conference on Sustainable Construction Materials and Technologies, Ancona, Italy, 28–30 June 2010; Zachar, J., Claisse, P., Naik, T.R., Ganjiam, E., Eds.; UWM Center for By-Products Utilization: Milwaukee, WI, USA, 2010.
24. Marroccoli, M.; Montagnaro, F.; Pace, M.L.; Valenti, G.L. Use of fluidized bed combustion ash and other industrial wastes as raw materials for the manufacture of calcium sulphoaluminate cements. In Proceedings of the 20th International Conference on Fluidized Bed Combustion, Xian, China, 18–21 May 2009; Yue, G., Zhang, H., Zhao, C., Luo, Z., Eds.; Springer: Berlin, Heidelberg, Germany, 2009; pp. 389–395.
25. Chaunsali, P.; Vaishnav, K. Calcium-sulfoaluminate-belite cements: Opportunities and challenges. *Indian Concr. J.* **2020**, *94*, 18–25.

26. Telesca, A.; Marroccoli, M.; Winnefeld, F. Synthesis and characterisation of calcium sulfoaluminate cements produced by different chemical gypsums. *Adv. Cem. Res.* **2019**, *31*, 113–123. [CrossRef]
27. Zajac, M.; Skocek, J.; Stabler, C.; Bullerjahn, F.; Ben Haha, M.B. Hydration and performance evolution of belite–ye'elimite–ferrite cement. *Adv. Cem. Res.* **2019**, *31*, 124–137. [CrossRef]
28. Telesca, A.; Marroccoli, M.; Ibris, N.; Naik, T.R.; Lupiáñez, C.; Díez, L.I.; Romeo, L.M.; Montagnaro, F. Synthesis and characterization of belite calcium sulfoaluminate cements produced by oxyfuel combustion residues. In Proceedings of the 5th Sustainable Construction Materials and Technologies, Kingston upon Thames, UK, 14–17 July 2019; Ganjian, E., Claisse, P., Ghafoori, N., Limbchiya, M., Bagheri, M., Eds.; Volume 2. Code 149940.
29. Mobili, A.; Belli, A.; Giosué, C.; Telesca, A.; Marroccoli, M.; Tittarelli, F. Calcium sulfoaluminate, geopolimeric, and cementitious mortars for structural applications. *Environments* **2017**, *4*, 64. [CrossRef]
30. Álvarez-Pinazo, G.; Santacruz, I.; Aranda, M.A.G.; De La Torre, Á.G. Hydration of belite–ye'elimite–ferrite cements with different calcium sulfate sources. *Adv. Cem. Res.* **2016**, *28*, 529–543. [CrossRef]
31. Borštnara, M.; Daneuc, N.; Doleneca, S. Phase development and hydration kinetics of belite-calcium sulfoaluminate cements at different curing temperatures. *Cer. Int.* **2020**, *46*, 29421–29428. [CrossRef]
32. Shen, Y.; Qian, J. Utilization of phosphogypsum for sulfate-rich belite sulfoaluminate cement production. *Adv. Cem. Res.* **2015**, *27*, 515–525. [CrossRef]
33. Ma, B.; Li, X.; Shen, X.; Mao, Y.; Huang, H. Enhancing the addition of fly ash from thermal power plants in activated high belite sulfoaluminate cement. *Constr. Build. Mater.* **2014**, *52*, 261–266. [CrossRef]
34. Valenti, G.L.; Marroccoli, M.; Pace, M.L.; Telesca, A. Discussion of the paper 'Understanding expansion in calcium sulfoaluminate–belite cements' by Chen, I.A. et al., Cem. Concr. Res. **2012**, *42*, 51–60. *Cem. Concr. Res.* **2012**, *42*, 1555–1559. [CrossRef]
35. Chen, I.A.; Juenger, M.C. Incorporation of coal combustion residuals into calcium sulfoaluminate-belite cement clinkers. *Cem. Concr. Comp.* **2012**, *34*, 893–902. [CrossRef]
36. Irvin, A.C.; Juenger, M.C.G. Synthesis and hydration of calcium sulfoaluminate-belite cements with varied phase compositions. *J. Mat. Sci.* **2011**, *46*, 2568–2577. [CrossRef]
37. Cuberos, A.J.M.; De La Torre, A.G.; Martin-Sedeno, M.C.; Schollbach, K.; Pollmann, H.; Aranda, M.A.G. Active iron-rich belite sulfoaluminate cements: Clinkering and hydration. *Environ. Sci. Technol.* **2010**, *44*, 6855–6862. [CrossRef] [PubMed]
38. Pimraksa, K.; Hanjitsuwan, S.; Chindaprasirt, P. Synthesis of belite cement from lignite fly ash. *Ceram. Int.* **2009**, *35*, 2415–2425. [CrossRef]
39. Glasser, F.P.; Zhang, L. High-performance cement matrices based on calcium sulfoaluminate-belite compositions. *Cem. Concr. Res.* **2001**, *31*, 1881–1886. [CrossRef]
40. Quillin, K. Performance of belite-sulfoaluminate cements. *Cem. Concr. Res.* **2001**, *31*, 1341–1349. [CrossRef]
41. Arjunan, P.; Silsbee, M.R.; Roy, D.M. Sulfoaluminate-belite cement from low-calcium fly ash and sulfur-rich and other industrial by-products. *Cem. Concr. Res.* **1999**, *29*, 1305–1311. [CrossRef]
42. Gao, Y.; Li, Z.; Zhang, J.; Zhang, Q.; Wang, Y. Synergistic use of industrial solid wastes to prepare belite-rich sulphoaluminate cement and its feasibility use in repairing materials. *Constr. Build. Mater.* **2020**, *264*, 120201. [CrossRef]
43. Su, D.; Li, Q.; Guo, Y.; Yue, G.; Wang, L. Effect of residual $CaSO_4$ in clinker on properties of high belite sulfoaluminate cement based on solid wastes. *Materials* **2020**, *13*, 429. [CrossRef]
44. Galluccio, S.; Beirau, T.; Pollmann, H. Maximization of the reuse of industrial residues for the production of eco-friendly CSA-belite clinker. *Constr. Build. Mater.* **2019**, *208*, 250–257. [CrossRef]
45. Kiventerä, J.; Piekkari, K.; Isteri, V.; Ohenoja, K.; Tanskanen, P.; Illikainen, M. Solidification/stabilization of gold mine tailings using calcium sulfoaluminate-belite cement. *J. Clean. Prod.* **2019**, *239*, 118008. [CrossRef]
46. Julphunthong, P. Synthesizing of calcium sulfoaluminate-belite (CSAB) cements from industrial waste materials. *Mater. Today Proc.* **2018**, *5*, 14933–14938. [CrossRef]
47. Rungchet, A.; Poon, C.S.; Chindaprasirt, P.; Pimraksa, K. Synthesis of low-temperature calcium sulfoaluminate-belite cements from industrial wastes and their hydration: Comparative studies between lignite fly ash and bottom ash. *Cem. Concr. Comp.* **2017**, *83*, 10–19. [CrossRef]
48. El-Alfi, E.A.; Gado, R.A. Preparation of calcium sulfoaluminate-belite cement from marble sludge waste. *Constr. Build. Mater.* **2016**, *113*, 764–772. [CrossRef]

49. Xue, P.; Xu, A.; He, D.; Yang, Q.; Liu, G.; Engstrom, F.; Bjorkman, B. Research on the sintering process and characteristics of belite sulphoaluminate cement produced by BOF slag. *Constr. Build. Mater.* **2016**, *122*, 567–576. [CrossRef]
50. Rungchet, A.; Chindaprasirt, P.; Wansom, S.; Pimraksa, K. Hydrothermal synthesis of calcium sulfoaluminate-belite cement from industrial waste materials. *J. Clean. Prod.* **2016**, *115*, 273–283. [CrossRef]
51. Senff, L.; Castela, A.; Hajjaji, W.; Hotza, D.; Labrincha, J.A. Formulations of sulfobelite cement through design of experiments. *Constr. Build. Mater.* **2011**, *25*, 3410–3416. [CrossRef]
52. Ferone, C.; Capasso, I.; Bonati, A.; Roviello, G.; Montagnaro, F.; Santoro, L.; Turco, R.; Cioffi, R. Sustainable management of water potabilization sludge by means of geopolymers production. *J. Clean. Prod.* **2019**, *229*, 1–9. [CrossRef]
53. Ahmad, T.; Ahmad, K.; Alam, M. Sustainable management of water treatment sludge through 3'R' concept (Review). *J. Clean. Prod.* **2019**, *124*, 1–13. [CrossRef]
54. CEN. *EN 196-2. Method of Testing Cement-Part 2: Chemical Analysis of Cement*; CEN: Brussels, Belgium, 2013.
55. Taylor, H.F.W. *Cement Chemistry*, 2nd ed.; Thomas Telford: London, UK, 1997.
56. Bernardo, G.; Telesca, A.; Valenti, G.L. A porosimetric study of calcium sulfoaluminate cement pastes cured at early ages. *Cem. Concr. Res.* **2006**, *36*, 1042–1047. [CrossRef]
57. Winslow, D.N.; Diamond, S. A mercury porosimetry study of the evolution of porosity in Portland cement. *ASTM J. Mater.* **1970**, *3*, 564–585.
58. Garboczi, E.J. Permeability, diffusivity, and microstructural parameters: A critical review. *Cem. Concr. Res.* **1990**, *20*, 591–601. [CrossRef]